Chemistry & Biology, Vol. 12, 941–950, August, 2005, ©2005 Elsevier Ltd All rights reserved. DOI 10.1016/j.chembiol.2005.06.008

A Ribozyme for the Aldol Reaction

Stefan Fusz, Alexander Eisenführ, Seergazhi G. Srivatsan, Alexander Heckel, and Michael Famulok*
Universität Bonn
Kekulé-Institut für Organische Chemie und Biochemie
Gerhard-Domagk-Strasse 1
53121 Bonn, Germany

Summary

Directed in vitro evolution can create RNA catalysts for a variety of organic reactions, supporting the "RNA world" hypothesis, which proposes that metabolic transformations in early life were catalyzed by RNA molecules rather than proteins. Among the most fundamental carbon-carbon bond-forming reactions in nature is the aldol reaction, mainly catalyzed by aldolases that utilize either an enamine mechanism (class I) or a Zn^{2+} cofactor (class II). We report on isolation of a Zn^{2+}-dependent ribozyme that catalyzes an aldol reaction at its own modified 5′ end with a 4300-fold rate enhancement over the uncatalyzed background reaction. The ribozyme can also act as an intermolecular catalyst that transfers a biotinylated benzaldehyde derivative to the aldol donor substrate, coupled to an external hexameric RNA oligonucleotide, supporting the existence of RNA-originated biosynthetic pathways for metabolic sugar precursors and other biomolecules.

Introduction

According to the "RNA world" hypothesis, early history of life on earth involved a period in which chemical transformations were catalyzed exclusively by RNA molecules, which are capable of genetic function and are able to fold into complex three-dimensional shapes, like structured proteins [1, 2]. The fact that peptide bond formation in the ribosome is catalyzed by the RNA portion in the large subunit in all kingdoms of life supports this hypothesis, as it may represent an artifact of this RNA-dominated evolutionary period that is still present in today's biomolecules [3]. Other functional RNAs that can be found in present organisms also support this hypothesis. Among them are natural self-cleaving RNAs [2], components of the spliceosome [4], a ribozyme that can be triggered by a small metabolite [5], and the so-called riboswitch RNAs, which regulate bacterial metabolism by allosteric binding to small-molecule metabolites [6].

In vitro evolution experiments using random sequence RNA or DNA libraries provide another source of versatile nucleic acid catalysts. These experiments, carried out in the laboratory, can be viewed as a model of RNA evolution in the RNA world, and have led to a variety of RNAs that catalyze biologically important chemical reactions, such as nucleotide (nt) synthesis [7], redox reactions [8, 9], peptide- [10] and amide bond [11] formations and cleavage [12], amino acid ester transfer [13, 14] and aminoacylations [15–17], the Michael reaction [18], porphyrine metallations [19, 20], alkylations [21, 22], and RNA polymerizations [23]. The only known RNAs that catalyze carbon-carbon bond formations are ribozymes for the Diels-Alder reaction [24, 25].

Despite this rather broad scope of different metabolically relevant chemical transformations for which ribozyme examples exist, there are several important reactions that have not yet been carried out with a ribozyme. For example, identification of a ribozyme that catalyzes a substrate-specific aldol reaction would be a significant achievement because it would demonstrate the ability of RNA to accelerate a chemical reaction important in several biologically relevant metabolic transformations, particularly in nt synthesis, like the formation of ribose from simple aldehydes [1]. We therefore applied in vitro selection of a highly diverse RNA library, consisting of 2×10^{15} different sequences, to test whether RNA catalysts that are able to accelerate an aldol reaction between a levulinic amide aldol donor substrate and a biotinylated benzaldehyde-4-carboxamide derivative could be evolved.

Results and Discussion

The aldol reaction and the modified reactants investigated in this study are shown in Figure 1. We evolved the aldolase ribozyme by iterative cycles of in vitro selection [26–28] using a previously described 194 nt RNA library with two randomized regions of 70 and 72 nt, separated by a 14 nt constant region, and flanked by two constant primer binding sites [10, 18]. Each of the 2×10^{15} members of the library was 5′-modified with a levulinic amide aldol donor substrate via a flexible linker, including a photocleavable *o*-nitrobenzyl residue (**1**). The ketone substrate was attached to the 5′-monophosphate group of a guanosine monomer to yield **1a** (syntheses of substrates will be published elsewhere), which was used as an initiator nt during in vitro transcription of the library with T7 RNA polymerase. To select for RNA sequences capable of catalyzing the aldol reaction, the resulting pool was incubated with the biotinylated benzaldehyde-4-carboxamide substrate **2**. Thus, active sequences tagged themselves with biotin, resulting in a distinctive feature for separation of reacted and unreacted RNA by streptavidin agarose affinity chromatography (Figure 2A). To exclude the undesired enrichment of sequences that reacted at other potentially nucleophilic sites in the RNA, and to enforce the enrichment of sequences that yielded the aldol reaction product **3**, a photocleavable linker was attached to the ultimate 5′-phosphate group. Upon UV irradiation, the biotin tag is removed only from those sequences that have carried out the desired reaction, whereas sequences that bear the tag at other sites remain bound to the streptavidin matrix. As a control, we

*Correspondence: m.famulok@uni-bonn.de

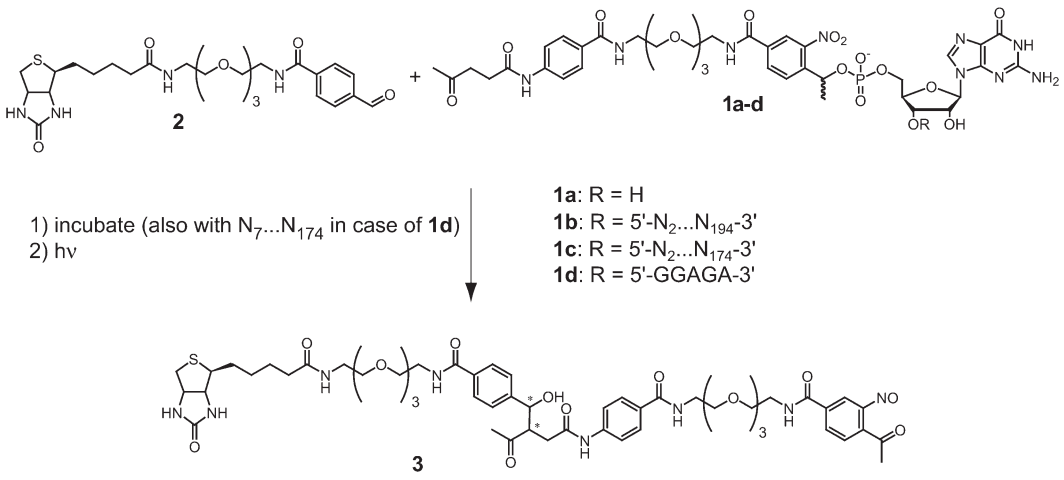

Figure 1. Ribozyme-Mediated Aldol Reaction and UV Release of the Product

The modified guanosine residue **1a** used in the in vitro transcription as well as the levulinic acid derivatives **1b–1d** and aldehyde **2**, which yield the aldol reaction product **3** (postulated thermodynamic regioisomer) after UV cleavage. **1b**: Levulinic acid-modified full-length ribozyme for the "in *cis*" reaction, **1c**: 3′-truncated 174 nt version of **1b**; **1d**: hexamer-substrate for the "in *trans*" reaction; substrate **1d** was also incubated with a ribozyme version consisting of nt N_7–N_{174}.

performed two selections in parallel, one in which reverse transcription and PCR amplification were performed directly on immobilized RNA sequences, the other one including the UV cleavage step (Figures 2A and 2B). We gradually increased the stringency of the selection by reducing the incubation time (Figure 2B). After 11 selection cycles, no further enrichment was achieved. Interestingly, enrichment was observed both in the UV cleavage and the direct amplification selection. We cloned and sequenced 21 samples from each selection and obtained, in each case, the same main family with sequences that varied only by point mutations in 19 different positions overall within the second randomized region, whereas the first randomized region showed only point mutations at three positions (Figure 3A and see Figure S1 in the Supplemental Data available with this article online). Clone 11D2, the most abundant (13 out of 21) and most active sequence (data not shown) from the direct amplification, was used for all further investigations. The highest number of point mutations found within one sequence compared to clone 11D2 was four. The point mutations do not appear to allude to a particular secondary structure motif.

Sequence Requirements and Secondary Structure of the 11D2 Ribozyme

To determine a minimal motif of the ribozyme, we synthesized different truncated versions of clone 11D2. We deleted several stretches of nt between positions N_7 and N_{99}, but left at least the first six nt and the 5′-modification unchanged. These deletions resulted in complete loss of activity (data not shown). In contrast, the ribozyme was much more tolerant of truncation from the 3′ end (Figure 3B). For example, a truncation of 20 nt containing the entire constant 3′-primer region maintained full activity. Further 3′-truncation led to a stepwise reduction of activity to 20% for $11D2_{1\text{-}111}$, and $11D2_{1\text{-}106}$ no longer exhibited any appreciable activity (4%). From these data we conclude that the catalytically active center is located between positions 1 and 111, whereas the following 63 nt play an important role in stabilizing an active conformation of the ribozyme.

The secondary structure of the ribozyme was investigated by enzymatic probing using RNase T_1, A, and V_1, and nuclease S_1. RNA for the structural probing was subjected to the same denaturing/refolding procedure as the RNA for the selection and the kinetic studies. The 5′-labeled RNA can only be generated without the 5′-ketone modification. The 3′-labeled RNA was probed both with and without the 5′-ketone modification. No significant difference was observed, indicating that this modification does not affect folding (data not shown). However, at present it is not clear what fraction of the ribozyme exists in an active form. Because RNAs may fold into different structures of similar energies—especially with increasing length—enzymatic probing will inherently give an overall picture of the secondary structure that shows the most abundant structural motifs, but may not necessarily represent the most active conformation.

Figures 4A and 4B show a representative probing gel at different time points during the gel run; Figure 4C presents the corresponding secondary structure that correlates best with the cleavage pattern obtained with the different nucleases. The color coding represents an average over five independent structural probing experiments. The structure is characterized by a series of hairpin loops and bulged hairpins that branch off from a single-stranded central sequence motif. The only detail that does not exactly fit with the secondary structure shown in Figure 4B is the involvement of the C^{13}-C^{14}-U^{15}-loop of the 5′-hairpin motif in double-strand formation, as indicated by the clear nuclease V_1 cleavage pattern obtained for these positions (Figure 4B). This suggests that the loop might be engaged in the forma-

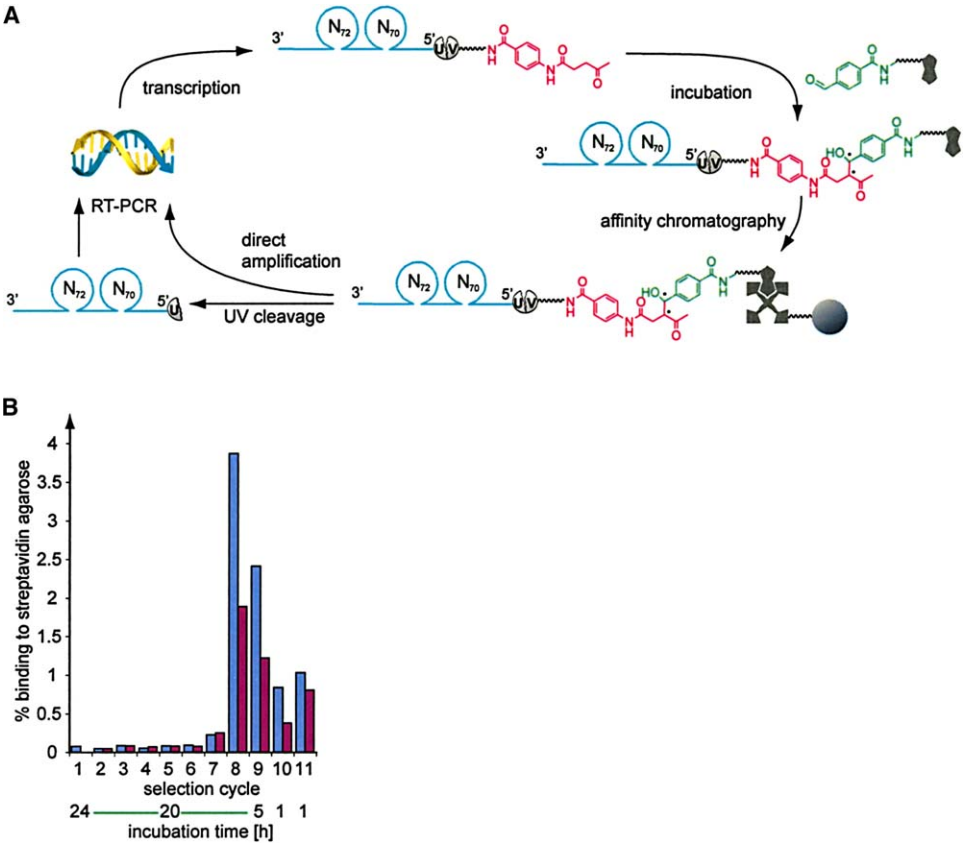

Figure 2. Selection of Ribozymes that Catalyze the Aldol Reaction

(A) Selection scheme: a levulinic acid-modified RNA-pool with constant and randomized regions as shown (see also Figure 1) was incubated with the biotinylated aldehyde **2** (green substrate). Reacted sequences were separated by affinity chromatography on streptavidin agarose (gray). RT-PCR was performed after UV cleavage, or directly with the loaded agarose beads, to obtain dsDNA. The enriched pool for the next selection cycle was obtained by transcription with the modified G residue **1a** as an initiator nt.

(B) Course of the selection cycles 1–11. Blue: direct amplification; magenta: amplification after UV cleavage. The stringency of the selection was increased in cycle 9 by reducing the incubation time from 20 to 5 hr, and in cycles 10 and 11 by further reduction to 1 hr incubation time.

tion of a pseudoknot structure. A candidate pairing motif would be A^{76}-G^{77}-G^{78}, for which we did not obtain any cleavage by the single-strand-specific nucleases (Figure 4C).

Clone 11D2 Requires Zn^{2+} Ions for Activity

Depending on the manner of aldol donor activation, protein aldolases are subdivided into two mechanistic classes. Class I aldolases lead to stereoselective deprotonation when the substrate is covalently attached to a lysine residue in the active site as a Schiff base. In contrast, class II aldolases require divalent metal ions, mainly Zn^{2+}, in the active site, which acts as a Lewis acid cofactor, polarizing the ketone group to facilitate deprotonation of the α-acidic position in the aldol donor and stabilizing the transition state [29, 30]. Due to the low nucleophilicity of the exocyclic primary amino groups in RNA bases, we considered it unlikely that we would be able to isolate RNAs that would utilize the class I mechanism. We therefore included 300 μM Zn^{2+} in the selection buffer to aim for class II-like aldolase ribozymes. Indeed, as shown in Figure 5A, the ribozyme is inactive in the absence of Zn^{2+} ions and reaches a plateau of activity at a concentration of 900 μM Zn^{2+} ions. In contrast, Mg^{2+} ions enhance the catalytic performance, with an optimal concentration of 10 mM, but are not explicitly required for activity. We could not detect any catalysis at 0 mM Zn^{2+} in presence of 10 mM Mg^{2+}, whereas at 0 mM Mg^{2+} in the presence of 900 μM Zn^{2+}, the ribozyme showed about 6% of the activity at the optimal ion concentrations, indicating that Zn^{2+} ions are essential for catalysis. The Zn^{2+} concentration for a half-maximal reaction rate $[Zn^{2+}]_{1/2}$ is 380 μM, the respective concentration for Mg^{2+} $[Mg^{2+}]_{1/2}$ is 2.6 mM. We compared this system, in which the RNA **1c** catalyzes the modification of its own 5′ end—the so-called "in *cis*" reaction—with a system in which the first six nt from the 5′ end of the ribozyme are removed to form an independent hexameric RNA aldol donor substrate containing the levulinic amide (**1d**) and are accepted as substrate by the shortened ribozyme $11D2_{7\text{-}174}$—the so-called "in *trans*" reaction. Identical respective values for the $[M^{2+}]_{1/2}$ were found for the "in *cis*" reaction and the "in *trans*" reaction, indicating that both ions do not appear to be essential for the binding of **1d** to the shortened ribozyme $11D2_{7\text{-}174}$.

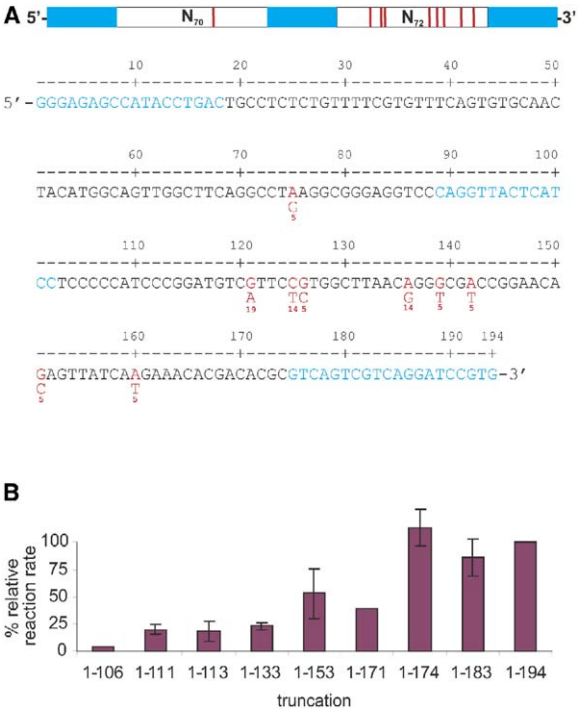

Figure 3. Sequence Variation of Selected Clones and Truncation of the Most Abundant Clone 11D2

(A) Upper panel. Blue boxes: constant regions; white boxes: randomized regions; red: sites of variation found in different clones. Lower panel: Primary sequence of the most abundant full-length ribozyme. The color scheme reflects that of the upper panel. Variations in different isolated sequences of the direct amplification are indicated in red with the percentage of their abundance given underneath.

(B) Relative reaction rates of the "in *cis*" reaction of different 3′-truncated versions relative to the full-length 1–194 ribozyme (100%). Unless otherwise noted, experiments have been performed in duplicate. Error bars represent 1 SD.

The sigmoidal shape of the curves in Figure 5A suggests that divalent metal ions are bound in a cooperative fashion. We therefore determined the Hill coefficients for both ions in the "in *cis*" and "in *trans*" reaction (Figure 5B). The self-modifying reaction of **1c** and the intermolecular reaction of **1d** both revealed similar Hill coefficients for Mg^{2+} (Mg^{2+}: n_{cis} = 1.2; n_{trans} = 1.3). Thus, Mg^{2+} ions do not appear to be bound cooperatively. In contrast, with Hill coefficients around 3.0 (Zn^{2+}: n_{cis} = 2.6; n_{trans} = 3.3), Zn^{2+} ions are bound cooperatively; the ribozyme probably contains three cooperative binding sites for Zn^{2+} ions.

We next investigated whether divalent metal ions other than Zn^{2+} would also be able to promote catalysis of the 11D2 ribozyme in a similar fashion. Figure 5C shows that, with 10 mM Mg^{2+}, the ribozyme was active only in the presence of 1 mM Zn^{2+}, whereas no product formation could be detected when the reaction was carried out at 10 mM Mg^{2+} in the presence of 1 mM Ca^{2+}, Sr^{2+}, Ba^{2+}, Mn^{2+}, Co^{2+}, Ni^{2+}, Cu^{2+}, Cd^{2+}, Hg^{2+}, $B(OH)_3$, or Al^{3+}, all used as metal chlorides, except for $Sr(NO_3)_2$, $CuSO_4$, and $B(OH)_3$. Similar results were obtained using a 5 mM concentration of the respective ions (data not shown). At 1 mM, both $ZnSO_4$ and $ZnCl_2$ promoted the reaction equally well, ruling out any influence of the anion. This metal ion fidelity of the 11D2 ribozyme is in contrast to protein aldolases. For example, L-rhamnulose-1-phosphate aldolase appears to be promiscuous with respect to certain divalent metal ions. Catalysis in this protein is promoted by Zn^{2+}, Ni^{2+}, Co^{2+}, Cu^{2+}, and Mn^{2+}, but not by ions such as Mg^{2+}, Ca^{2+}, Ba^{2+}, Cd^{2+}, and Al^{3+} [31].

Although the strict requirement of Zn^{2+} ions in our ribozyme suggests that they exhibit an active role in the catalytic step, it is also possible that the ribozyme requires Zn^{2+} simply to support its folding and to stabilize its structure. The number of cooperatively bound ions does not allow any conclusions about the absolute number of bound ions (other than the lower limit). A possibility consistent with (but not demanded by) the data is that the catalytic mechanism of the ribozyme includes the formation of a scaffold that positions a Zn^{2+} ion cofactor in the active site to enable deprotonation of the aldol donor, similar to the mechanism of the class II protein aldolases [30]. Thus, the fact that cooperativity was found for Zn^{2+} ions but not for Mg^{2+} ions does not exclude the possibility that Mg^{2+} ions might somehow participate in the catalytic step of the reaction. Identifying the exact role of Mg^{2+} and Zn^{2+} ions in the catalytic strategy of this ribozyme will be an important direction for future research.

Kinetic Characterization of the 11D2 Ribozyme

For kinetic characterization, we used the truncated 1–174 nt version of clone 11D2 (**1c** in Figure 1) and first investigated the self-modifying "in *cis*" reaction of **1c** (Figure 6A). The ^{32}P-radiolabeled ketone-modified RNA **1c** was incubated with different concentrations of the aldehyde **2**. Aliquots were drawn at different incubation times, and product yields were determined by determining the percentage of biotinylated ribozyme after elution from a streptavidin matrix. The integrity of this product was confirmed by gel electrophoresis: the right panel of Figure 6A shows the transcribed 5′-modified ribozyme before (lane 1) and after (lane 2) UV cleavage in comparison with the product of the "in *cis*" reaction after purification on streptavidin agarose, followed by elution with formamide, before (lane 3) and after UV cleavage (lane 4). The finding that the mobility of the reaction product (lane 3) decreases compared to that of the unreacted modified ribozyme (lane 1) shows that the molecule has reacted with the aldehyde **2** and that molecular weight has been added to the product. After UV cleavage, products of the same lengths are obtained for the unreacted (lane 2) and the reacted modified ribozyme (lane 4), clearly showing that the reaction must have occurred at the 5′ modfication and not at the nucleic acid part of the ribozyme. This is further supported by negative control experiments in which either the RNA 5′ end was unmodified or in which the biotinylated aldehyde **2** was left out. In both cases, no immobilization on streptavidin agarose was observed (data not shown).

Figure 6A, left panel, shows the dependence of the initial reaction rate on the concentration of the aldehyde substrate **2**. The ribozyme exhibited an enzyme-like be-

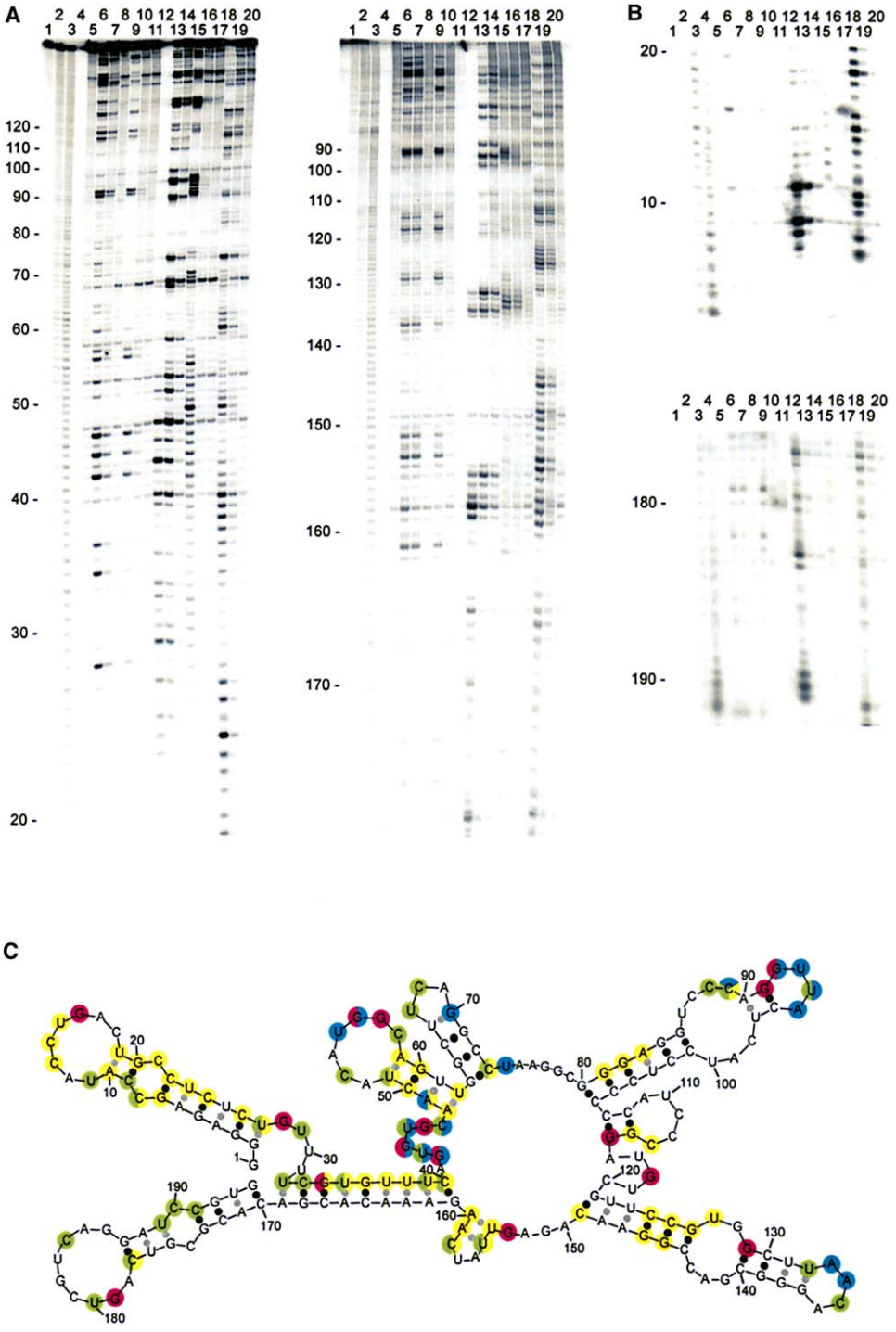

Figure 4. Sequence and Secondary Structure of Clone 11D2

(A) Representative probing gels. In the left gel, the RNA is 5′-^{33}P-labeled; in the right gel, it is 3′-^{33}P-labeled. The numbers on the vertical axis show the nt position. In both gels, the lanes are as follows: (1) control lane; (2–4) alkaline hydrolysis ladder (incubation for 2/5/15 min); (5–7) denaturing RNase T_1 ladder (0/1/10 U/ml); (8) reference lane—RNA in probing buffer without any nuclease; (9–11) RNase T_1 (0.1/1.0/10.0 U/ml); (12–14) RNase A (0.001/0.010/0.100 μg/ml); (15–17) nuclease S_1 (0.01/0.10/1.00 U/μl); (18–20) RNase V_1 (0.01/0.10/1.00 U/ml).

(B) The same set of samples after decreased duration of the gel running time to resolve shorter fragments below 20 or above 180 nt in length, respectively. The numbering is the same as in (A). Upper panel: 5′-^{33}P-labeled RNA; lower panel: 3′-^{33}P-labeled RNA.

(C) Proposed secondary structure of the ribozyme $11D2_{1\text{-}194}$ (**1b**). This secondary structure matches best with enzymatic probing data. The colors represent cleavage sites with the following enzymes: RNase T_1 (pink, specific for single-stranded G residues); RNase A (green, specific for single-stranded C/U residues); nuclease S_1 (blue, specific for single-stranded RNA); and RNase V_1 (yellow, specific for double-stranded RNA). Results were averaged over five independent experiments.

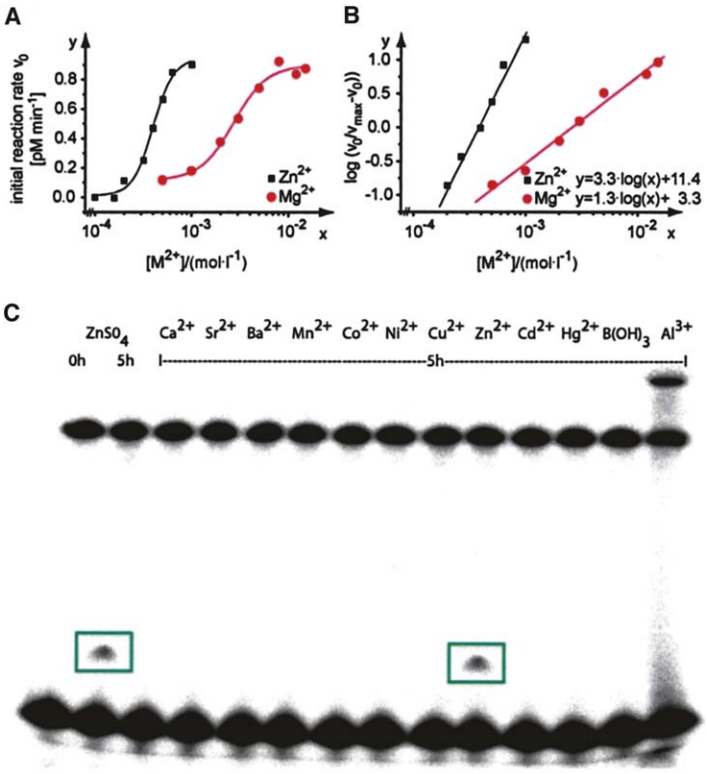

Figure 5. Influence of the Divalent Ions on the Initial Rate of Product Formation in the "in *trans*" Reaction

(A) Initial rate, v_0, as a function of the concentrations of Zn^{2+} (at 10 mM Mg^{2+}) and Mg^{2+} (at 0.8 mM Zn^{2+}).

(B) Hill-plot derived from the data shown in (A). Zn^{2+} is required for catalysis, whereas Mg^{2+} is not. In the absence of Zn^{2+}, Mg^{2+} does not support any catalytic activity, whereas Zn^{2+} alone does. From the Hill plots, a Hill coefficient of n = 3.3 for Zn^{2+} (with $[Zn^{2+}]_{1/2}$ =0.38 mM) and of n = 1.3 for Mg^{2+} (with $[Mg^{2+}]_{1/2}$ =2.55 mM) was determined. The "in *cis*" reaction gave similar results: n = 2.6 for Zn^{2+} (with $[Zn^{2+}]_{1/2}$ =0.30 mM), and n = 1.2 for Mg^{2+} (with $[Mg^{2+}]_{1/2}$ = 2.21 mM).

(C) M^{2+} and M^{3+} substitutions of Zn^{2+}. Shown is the influence of different salts on aldol product formation in the reaction with the hexameric substrate **1d**. In all experiments, the concentration of Mg^{2+} was set to 10 mM, whereas the concentration of Zn^{2+}, or that of the other indicated metal ions replacing Zn^{2+}, respectively, was set to 1 mM. Upper band: truncated ribozyme $11D2_{7\text{-}174}$; boxed middle: aldol product band; bottom band: ketone-modified hexameric RNA substrate **1d**. Al^{3+} causes partial precipitation of the RNA. First two lanes: $ZnSO_4$ after 0 and 5 hr. Except for $Sr(NO_3)_2$, $CuSO_4$, and $B(OH)_3$, the respective chlorides were used. $ZnCl_2$ was included to rule out any influence of the SO_4^{2-} ion or additional Cl^- ions on reaction rate. Thus, it could be shown that only Zn^{2+} supports product formation.

havior for the "in *cis*" reaction, going into saturation with increasing substrate concentrations. An apparent dissociation constant, K_M, of 1 mM was obtained for the enzyme-substrate complex of the biotinylated aldehyde **2** (Figure 6E). The "turnover number," k_{cat}, was determined to be 5.5 ± 0.7 × 10^{-4} min^{-1} (mean ± error propagation based on SD of the initial data), resulting in a specificity constant, k_{cat}/K_M, of 0.6 ± 0.1 M^{-1} min^{-1} (for more detailed information of kinetic characterization, see Figure S2). For comparison, the rate of product formation in the uncatalyzed background reaction was measured using the ketone-modified hexameric RNA **1d**, resulting in a k_{uncat} of 1.28 ± 0.09 × 10^{-4} M^{-1} min^{-1}. A similar experiment with modified starting pool **1b** produced the same results. Thus, the ribozyme **1c** showed a 4300-fold rate enhancement over the uncatalyzed background reaction.

The K_M of our ribozyme is in the same range as that of other biological aldol catalysts, such as the class I enzyme fructose-1,6-diphosphate-aldolase from mammals, with a K_M of 0.3–1.0 mM (depending on the tissue [32]) for the natural substrate D-glycerinaldehyde-3-phosphate and dihydroxyacetone phosphate. Other catalysts for the aldol reaction, which utilize a mechanism common to natural class I aldolases, are the catalytic antibodies 38C2 and 33F12 [33, 34], obtained through immunization in vivo. They are commercially available and enhance the formation of aldol products and, in certain cases, also of condensation products with a broad acceptance for aldol donors and acceptors. The K_M for the aldol donor/acceptor pair (acetone/4-acetamido benzaldehyde) that is most similar to the one used in this study is 0.204 mM—only 5-fold lower than the one found for our ribozyme **1c**, and the k_{cat} value of 480 × 10^{-4} min^{-1} is only 90-fold higher than in our system [34].

To study whether clone 11D2 can also catalyze the reaction on an external aldol donor substrate in an intermolecular reaction, we prepared a truncated version of this ribozyme that lacked the first six nt at the 5′ end ($11D2_{7\text{-}174}$). The corresponding hexameric RNA substrate **1d** was synthesized with the 5′-ketone modification by in vitro transcription and subjected to reaction with the aldehyde **2** in presence of $11D2_{7\text{-}174}$ under single-turnover conditions. The formation of the aldol product was followed by gel-shift of the ^{32}P-radiolabeled hexameric RNA substrate (Figure 6B). As before, we determined the initial reaction rates at different concentrations of aldehyde **2** and obtained the kinetic parameters applying the Michaelis-Menten equation (Figure 6E). Interestingly, the "in *trans*" reaction showed a K_M of 1 mM for **2**, which is similar to the one found for the "in *cis*" reaction. This indicates that the binding site for **2** in the truncated ribozyme $11D2_{7\text{-}174}$ is not significantly altered compared to the clone $11D2_{1\text{-}174}$, because the affinity for the biotinylated aldehyde **2** remains unchanged. Comparing the respective k_{cat} values, however, we found that the "in *trans*" reaction ex-

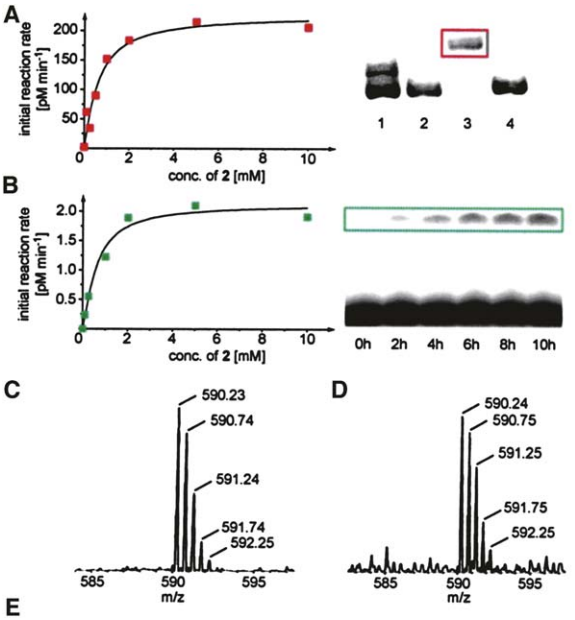

E

	'in cis' reaction	'in trans' reaction
K_M [mM]	1.0 ± 0.2	0.93 ± 0.09
v_{max} [pM min^{-1}]	274 ± 33	2.5 ± 0.2
k_{cat} [min^{-1}]	(5.5 ± 0.7) • 10^{-4}	(1.3 ± 0.1) • 10^{-5}
k_{cat} / K_M [M^{-1} min^{-1}]	0.6 ± 0.1	0.014 ± 0.002
k_{uncat} [M^{-1} min^{-1}]	(1.28 ± 0.09) • 10^{-4}	
(k_{cat} / K_M) / k_{uncat} (rate enhancement)	4300 ± 1000	109 ± 16

Figure 6. Kinetic Performance and Product Characterization

(A) Left: Michaelis-Menten plot of the "in *cis*" reaction. Right: denaturing PAGE gel-shift experiment; the transcription product (5′-modified ribozyme) before (lane 1) and after (lane 2) irradiation with UV light and the product of the "in *cis*" reaction after purification on streptavidin agarose, also before (lane 3) and after (lane 4) irradiation with UV light.

(B) Left: Michaelis-Menten plot of the "in *trans*" reaction. Right: denaturing PAGE gel-shift experiment; samples of the "in *trans*" reaction containing 1 mM aldehyde **2** after the given reaction time. The boxed product was quantified by phosphorimaging and used for the determination of the reaction rate.

(C) ESI-MS (with resolved isotope pattern) of the reaction product (red box in [A]) of the "in *cis*" reaction after photocleavage (expected mass: $[M + 2Na]^{2+}$, 590.25).

(D) The same mass is found for the "in *trans*" reaction product (green box in [B]).

(E) Kinetic parameters of the "in *cis*" and the "in *trans*" reaction. All error terms were calculated using error propagation, based on SD of the initial data.

hibited a 40-fold lower k_{cat} than the "in *cis*" reaction, resulting in a specificity constant, k_{cat}/K_M, of 0.014 ± 0.002 M^{-1} min^{-1}. The marked differences in the k_{cat} values are probably a consequence of the additional effect of the association characteristics of the hexameric substrate **1d** to the ribozyme $11D2_{7\text{-}174}$.

The 11D2 Ribozyme Catalyzes an Aldol Reaction

To further characterize the product formed in the "in *cis*" and "in *trans*" reactions, we purified the boxed products shown in Figure 6 by affinity chromatography on streptavidin agarose. Bound reaction products were eluted and precipitated with ethanol. For analytical detection of the formed product, we took advantage of the photocleavage site (Figure 2A). After UV irradiation, we subjected the respective samples to electrospray ionization time-of-flight mass spectrometric (ESI-TOF-MS) (positive mode) analysis. Both in the "in *cis*" (Figure 6C) and the "in *trans*" reaction (Figure 6D), the same peak was obtained that corresponds to the expected mass ($[M+2Na]^{2+}$) of the aldol product **3**. Without UV irradiation, the mass spectra of the same samples did not show the ions corresponding to the aldol product. As a negative control, we performed the same set of experiments using the unselected RNA from the starting pool instead of the ribozyme. In both cases, no aldol product was observed in the mass spectra (data not shown).

To further support the hypothesis that the ribozyme catalyzes an aldol reaction, and to evaluate its substrate specificity, we synthesized a set of derivatives of

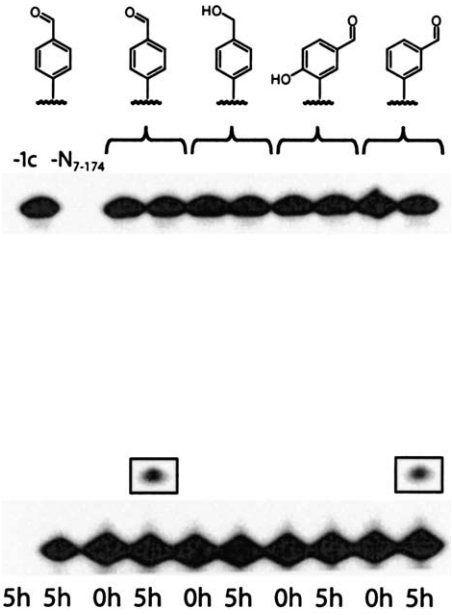

Figure 7. Substrate Specificity for the Ribozyme-Mediated Aldol Reaction

Substrate specificity for the ribozyme mediated aldol-reaction. Shown are different derivatives of aldehyde **2** used in an "in *trans*" reaction. Upper band: truncated ribozyme $N_{7\text{-}174}$ ($11D2_{7\text{-}174}$); boxed middle band: aldol product; lowest band: ketone-modified hexameric RNA substrate **1d**. The first two lanes on the left represent negative controls of the regular reaction containing the aldehyde **2** but lacking substrate **1d** or the ribozyme $N_{7\text{-}174}$ after 5 hr reaction time. The next two lanes represent the positive control with the parasubstituted aldehyde **2** after 0 and 5 hr, respectively. The subsequent lanes represent reactions with the shown derivatives after 0 and 5 hr. The benzyl alcohol derivative lacking the reactive aldehyde showed no product formation. The same result was found for the 5-formyl salicylic amide. The metasubstituted benzaldehyde yields 77% of product compared to **2**. Initial velocities were determined in triplicate gel-shift experiments for the "in *trans*" reaction, and are in good agreement with those obtained for the reaction with ribozyme **1c** (data not shown).

substrate **2** and investigated whether they are accepted by the ribozyme in both the "in *cis*" and the "in *trans*" reaction. Figure 7 shows the data for the intermolecular reaction in which the aldol-donor-derivatized hexamer-oligonucleotide substrate **1d** was used to react with the respective derivatives of compound **2**, catalyzed by ribozyme $11D2_{7\text{-}174}$. Consistent with the requirement of the aldehyde group, no reaction product appeared when we used a derivative of compound **2**, in which the aldehyde had been reduced to an alcohol. An isomer of compound **2**, in which the aldehyde was in meta- rather than paraposition, was accepted as a substrate, but yielded only 77% of the amount of product obtained with the progenitor parasubstrate used in the selection. This result indicates that the ribozyme tolerates a certain variation in the substrate structure. However, a substrate containing an additional OH group in the 5 position of the metaderivative of compound **2** was not accepted by the ribozyme and resulted in no product formation.

These data provide additional indirect evidence that the ribozyme catalyzes the transfer of the aldehyde substrate **2** to the levulinic acid substrates **1c–1d**, in accordance with an aldol reaction. The ketone substrate contains two potential sites for deprotonation: namely, the protons at the methyl- and methylene group next to the keto function. At present, we do not yet know which of the two sites is deprotonated, nor whether the aldol reaction occurs in a stereoselective fashion. The rather unreactive proton at the β-carbon adjacent to the amide moiety is unlikely to be the site of deprotonation.

Conclusion

We have selected a ribozyme that catalyzes an aldol reaction between a levulinic amide aldol donor and a benzaldehyde-4-carboxamide substrate. The only known RNAs that catalyze carbon-carbon bond formations are ribozymes for the Diels-Alder reaction [35]. Given the eminent relevance of the aldol reaction as a carbon-carbon bond-forming reaction in nature that plays a central role in cellular metabolism, the aldolase ribozyme described here fills an important gap and further supports the hypothesis of complex ribozyme-catalyzed metabolic pathways in the RNA world. Our ribozyme is only active in the presence of Zn^{2+}, like natural class II aldolases. Considering the ability of RNA to bind compounds as small as glycine [36], it can be envisioned that other ribozymes that utilize amino acids such as proline or lysine as cofactors could be selected. Because proline alone can catalyze stereospecific aldol reactions via enamine intermediates [37, 38], RNA selections aiming toward this end would pave the way to ribozymes with a mechanism similar to that of class I aldolases.

Significance

The first example of a ribozyme that catalyzes an aldol reaction is described. The ribozyme shows, for a self-modifying reaction, a 4300-fold rate enhancement over the uncatalyzed background reaction. Furthermore, we show that it can act as an intermolecular catalyst that transfers a biotinylated benzaldehyde derivative to the aldol donor substrate, coupled to an external hexameric RNA oligonucleotide. Our ribozyme is only active in the presence of Zn^{2+}, as also found for natural class II aldolases. The finding that RNA can catalyze aldol reactions supports the existence of RNA-originated biosynthetic pathways of many metabolic precursors of sugars and other biomolecules before modern cells arose. The ribozyme demonstrates that an RNA is, in principle, able to accelerate chemical reactions important in several biologically relevant metabolic transformations, particularly in nucleotide synthesis, such as the formation of ribose from simple aldehydes.

Experimental Procedures

Detailed information on the synthesis of ketone-modified guanosine **1a** and biotin aldehyde **2** will be published elsewhere. Given concentrations of **1b–1d** always refer to the ketone-modified portion.

Preparation of the RNA Pool

The previously reported [10, 18] DNA pool 5′-AGC GAA TTC TAA TAC GAC TCA CTA TAG GGA GAG CCA TAC CTG AC N_{70} CAG GTT ACT CAT CC N_{72} GTC AGT CGT CAG GAT CCG TG-3′ was used for the selection. For in vitro transcription, 10.2 nmol of PCR-amplified DNA was used in a 12 ml transcription reaction with 40 mM Tris-HCl (pH 8.0), 8 mM $MgCl_2$, 50 mM NaCl, 2 mM spermidine, 30 mM dithiothreitol, 3.5 mM ATP, CTP, and UTP, 1.5 mM GTP (Roche), 2 mM initiator nt **1a**, 13.2 nM [α-^{32}P]GTP (10 μCi/μl, Perkin-Elmer), 0.8 U/μl RNasin (Promega), 0.0004 U/μl inorganic pyrophosphatase (Roche), 0.6 U/μl T7 RNA polymerase (Stratagene), and transcribed for 12 hr at 37°C. RNA was purified on a 5% denaturing polyacrylamide gel, visualized (UV shadowing), excised, eluted (0.3 M NaOAc), EtOH-precipitated, and used for selection. In a PAGE assay, the ratio of ketone-modified RNA to nonmodified RNA was determined to be 49:51.

In Vitro Selection

In vitro selection was performed with a diversity of approximately 2×10^{15} in the starting pool and an average of three copies of every individual 5′-ketone-modified RNA. The RNA library was denatured at 94°C for 5 min in Mg^{2+}- and Zn^{2+}-free selection buffer B1, containing 150 mM NaCl, 50 mM K-HEPES (pH 7.4). The RNA was then cooled to 25°C for 10 min and then added to a mixture of selection buffer B2 containing the final concentrations of 5 mM $MgCl_2$, 0.3 mM $ZnSO_4$, 7% DMSO, 150 mM NaCl, 50 mM K-HEPES (pH 7.4), and 2 mM biotin aldehyde **2** to give a 0.5 μM solution. After incubation for 24 hr at room temperature, the reaction was stopped by ethanol precipitation. The pellet was dissolved in 1/2 of the former reaction volume and ethanol-precipitated again to remove traces of biotin aldehyde **2**. The stringency of the selection was gradually increased by decreasing the incubation time from 20 hr (cycles 2–8) to 5 hr (cycle 9) to 1 hr (cycles 10–11). RNA was dissolved in 800 μl streptavidin binding buffer (SAv-bb; 50 mM K-HEPES, 150 mM NaCl, 2 mM EDTA [pH 7.4]) and incubated with 20 μl streptavidin-agarose (SAv-agarose, Pierce) for 45 min at room temperature in Poly-Prep Chromatography Columns (BioRad) under shaking at 1000 rpm. The agarose was washed with 120 column volumes (CV) of SAv-bb, 80 CV denaturing buffer 1 M (50 mM K-HEPES, 150 mM NaCl, 5 mM EDTA, 1 M guanidinium·HCl, 0.05% [v/v] Triton X-100 [pH 7.9]) and 200 CV denaturing buffer 2 M (50 mM K-HEPES, 150 mM NaCl, 5 mM EDTA, 2 M guanidinium·HCl, 0,05% [v/v] Triton X-100 [pH 7.9]) in an alternating pattern, and finally with 50 CV SAv-bb and 10 CV H_2O. RNAs linked to SAv-agarose were reverse-transcribed directly using SuperScript II (Invitrogen), and PCR-amplified using Taq DNA polymerase (Promega) according to manufacturers' instructions. Beginning with cycle 2, a second selection (UV selection) was performed in parallel using the DNA of the first selection cycle. For this selection, the RNA was eluted from the agarose beads by exposing the sample to UV light at 366 nm in SAv-bb for 3 hr at 4°C using a 15 W UV-lamp. After washing with 2×5 CV H_2O and pooling the flow-through and the wash fractions,

the RNA was ethanol-precipitated and subjected to reverse transcription and PCR-amplification. Pool DNA from cycle 11 was cloned using the pGEM-T vector system (Promega) following the manufacturer's instructions and sequenced (SEQLAB, Göttingen, Germany). 3′- and 5′-truncations of the sequence 11D2 were obtained using appropriate primers during PCR amplification.

Structural Characterization of the Ribozyme 11D2$_{1-194}$ by Enzymatic Probing

In vitro-transcribed RNA was 5′- or 3′ end-labeled using [γ-^{33}P]ATP (10 μCi/μl; MP Biomedicals), polynucleotide kinase (Stratagene), T4 RNA ligase (NEB), and cytidine 3′-monophosphate (Sigma). RNA was refolded in 10 mM Tris-HCl (pH 7.4) with 100 mM KCl and 1 μg/μl yeast tRNA, subsequently adjusting the buffer to 10 mM $MgCl_2$. Reactions were augmented with 300 mM NaCl (for T_1 digests) or 280 mM NaCl and 4.5 mM $ZnCl_2$ (for S_1 digests). Parallel probing reactions employed three 10-fold nuclease dilutions starting from 0.01 U/μl RNase T_1 (Roche), 0.1 μg/ml RNase A (Sigma), 1 U/μl nuclease S_1 (Amersham), and 0.001 U/μl RNase V_1 (Ambion), respectively, and were incubated for 5 min at room temperature. Denaturing reactions with RNase T_1 were performed in CEU buffer (20 mM sodium citrate [pH 5.0], 1 mM EDTA, 7 M urea). Reactions were stopped by the addition of inactivation buffer (Ambion) and the RNA was ethanol-precipitated and separated on a denaturing 12% polyacrylamide gel. Gels were analyzed by phosphorimaging (Fujifilm FLA-3000). The results from five independent experiments were averaged and used for refinement of structures predicted by the mfold program [39].

Cooperativity Tests

Cooperativity tests were performed as described below in Kinetic Assays, with a fixed concentration of 2 mM aldehyde **2**. For the assay, one metal ion was held at the concentration at which reaction velocity reaches saturation (Zn^{2+}: 0.8 mM; Mg^{2+}: 10 mM), whereas the other metal ion was varied from 0 to 0.9 mM for Zn^{2+} and 0 to 15 mM for Mg^{2+}, respectively. At 5 different time points (0–5 hr), 20 μl aliquots of the 105 μl "in *cis*" reaction were taken and analyzed by immobilization on SAv-agarose. For the "in *trans*" reaction, 15 μl aliquots of the 85 μl reaction were taken at 5 different time points (0–6 hr), mixed with denaturing PAGE-stop buffer, and quantified by gel-shift on a 20% polyacrylamide gel.

From these data, the initial rate was determined. The v_{max} value was estimated to be 5% higher than the highest determined v_0. Cooperativity was determined from the Hill equation (1):

$$\log \frac{v_0}{(v_{max} - v_0)} = n\log[M^{2+}] - n\log K_D \quad (1)$$

Kinetic Assays

An optimized selection buffer (50 mM K-HEPES [pH 7.4], 150 mM NaCl, 15 mM $MgCl_2$, 0.8 mM $ZnSO_4$, 7% DMSO) was used in all kinetic experiments. For the "in *cis*" reaction, α-^{32}P-labeled clone 11D2$_{1-174}$ RNA (**1c**, 0.5 μM and 0.52 μM nonmodified RNA) was denatured and incubated at 25°C in a 210 μl reaction with concentrations of biotin aldehyde **2** ranging from 0 to 10 mM. At 10 different time points (0–8 hr), 20 μl aliquots were taken and the reaction stopped by ethanol precipitation. After a second ethanol precipitation, samples were dissolved in 200 μl SAv-bb and incubated for 45 min at room temperature with 10 μl of settled SAv-agarose. After extensive washing, according to the procedure described in the section In Vitro Selection, the fraction of bound RNA was measured by counting the radioactivity in a scintillation counter (Perkin-Elmer). From these data, the initial rate was determined, taking into account the ratio of modified RNA **1c** and unmodified RNA. The hexameric RNA **1d** was synthesized by in vitro transcription, using appropriate double-stranded DNA containing the T7 promoter. For the "in *trans*" reaction, 1 μM ribozyme 11D2$_{7-174}$ was denatured in the presence of 0.2 μM α-^{32}P-labeled hexameric ketone-modified RNA substrate **1d** in divalent ion-free selection buffer B1 and cooled to 25°C as described previously here. After addition of the divalent ions and DMSO (see above), the 95 μl reaction mixture was incubated at an optimized temperature of 20°C with various concentrations of biotin aldehyde **2** (0–10 mM). At 6 different time points (0–10 hr), 15 μl aliquots were taken, immediately mixed with denaturing PAGE-stop buffer (80% formamide, 20 mM EDTA), and stored at –80°C before loading on a denaturing 20% polyacrylamide gel. Quantification of the gel-shifted reaction product by phosphorimaging was used to determine the initial rates. The kinetic parameters for both reactions were calculated based on the Michaelis-Menten equation by curve-fitting from a Lineweaver-Burk plot (Origin 6.1 software). Errors were calculated using error propagation. The uncatalyzed background reaction was determined using the "in *trans*" system in a time range of 10 days at 25°C, replacing the ribozyme 11D2$_{7-174}$ with 1 μM catalytically inactive zero-round pool RNA **1b**.

M^{2+} and M^{3+} Substitution of Zn^{2+}

In a previously described reaction with substrate **1d** and the 11D2$_{7-176}$ ribozyme, the concentration of Mg^{2+} was set at 10 mM, whereas the concentration of Zn^{2+} (or the indicated other metal ions replacing Zn^{2+}) was set at 1 mM. For all samples, a 20 μl aliquot was taken after 5 hr reaction time, except for $ZnSO_4$, for which an additional aliquot was sampled at 0 hr. Except for $Sr(NO_3)_2$, $CuSO_4$, and $B(OH)_3$, the respective chlorides were used. All experiments were done in duplicate.

ESI-MS Analyses

Aldol products for both the "in *cis*" and the "in *trans*" reactions were obtained by following the incubation procedure and purification on SAv-agarose as previously described here. For the "in *cis*" reaction, 6 nmol of ketone-modified RNA 11D2$_{1-174}$ (**1c**, 0.5 μM final concentration) were used and incubated for 6 hr with 5 mM biotin aldehyde **2** and purified on 30 μl settled SAv-agarose. For the "in *trans*" reaction, 5 nmol of hexameric RNA substrate **1d** and 10 nmol ribozyme 11D2$_{7-174}$ were used at concentrations of 1 μM and 2 μM, respectively, and incubated for 42 hr with 2 mM biotin aldehyde **2** at 20°C. Quantitative precipitation was achieved by doubling the amount of ethanol added. Separation was done using 15 μl settled SAv-agarose. After the final washing step, the agarose-bound reaction product was eluted by heating for 5 min to 94°C in 2 CV of formamide elution buffer (98% formamide, 10 mM EDTA). The SAv-agarose was washed with 2 × 1 CV formamide elution buffer and 2 × 3 CV H_2O. The pooled eluates and wash fractions were ethanol-precipitated in the presence of 0.15 M NaOAc (pH 5.4). The "in *cis*" product was dissolved in 40 μl H_2O (20 μl for "in *trans*" product). A 5 μl aliquot of each sample was UV-irradiated at 366 nm for 5 min at room temperature. Samples before and after irradiation were diluted to 50% aqueous acetonitrile, before measuring ESI-TOF-MS in the positive ion mode on a Q-TOF 2 mass spectrometer (Micromass) equipped with a nanospray source (injection by glass capillary, long type, Protana, Odense, Denmark; capillary voltage of 1000 V, cone voltage 50–70 V). Instrument calibration was carried out with a mixture of sodium iodide and cesium iodide dissolved in 50% aqueous acetonitrile.

Supplemental Data

Supplemental Data, including additional data and figures, are available at http://www.chembiol.com/cgi/content/full/12/8/941/DC1/.

Acknowledgments

We thank Heike Hupfer for excellent technical assistance in measuring ESI-TOF-MS. This work was supported by the priority program "Directed Evolution of Biocatalysis" of the Deutsche Forschungsgemeinschaft. S.F., A.E., and A.H. thank the Fonds der Chemischen Industrie for fellowships. S.G.S. is grateful to the Alexander von Humboldt Foundation for a fellowship.

Received: May 1, 2005
Revised: June 11, 2005
Accepted: June 13, 2005
Published: August 26, 2005

References

1. Joyce, G.F. (2002). The antiquity of RNA-based evolution. Nature *418*, 214–221.

2. Doudna, J.A., and Cech, T.R. (2002). The chemical repertoire of natural ribozymes. Nature *418*, 222–228.
3. Ban, N., Nissen, P., Hansen, J., Moore, P.B., and Steitz, T.A. (2000). The complete atomic structure of the large ribosomal subunit at 2.4 Å resolution. Science *289*, 905–920.
4. Valadkhan, S., and Manley, J.L. (2001). Splicing-related catalysis by protein-free snRNAs. Nature *413*, 701–707.
5. Winkler, W.C., Nahvi, A., Roth, A., Collins, J.A., and Breaker, R.R. (2004). Control of gene expression by a natural metabolite-responsive ribozyme. Nature *428*, 281–286.
6. Winkler, W.C., and Breaker, R.R. (2003). Genetic control by metabolite-binding riboswitches. Chembiochem *4*, 1024–1032.
7. Unrau, P.J., and Bartel, D.P. (1998). RNA-catalysed nucleotide synthesis. Nature *395*, 260–263.
8. Tsukiji, S., Pattnaik, S.B., and Suga, H. (2003). An alcohol dehydrogenase ribozyme. Nat. Struct. Biol. *10*, 713–717.
9. Tsukiji, S., Pattnaik, S.B., and Suga, H. (2004). Reduction of an aldehyde by a NADH/Zn^{2+}-dependent redox active ribozyme. J. Am. Chem. Soc. *126*, 5044–5045.
10. Zhang, B., and Cech, T.R. (1997). Peptide bond formation by in vitro selected ribozymes. Nature *390*, 96–100.
11. Wiegand, T.W., Janssen, R.C., and Eaton, B.E. (1997). Selection of RNA amide synthases. Chem. Biol. *4*, 675–683.
12. Dai, X., De Mesmaeker, A., and Joyce, G.F. (1995). Cleavage of an amide bond by a ribozyme. Science *267*, 237–240.
13. Lohse, P.A., and Szostak, J.W. (1996). Ribozyme-catalysed amino-acid transfer reactions. Nature *381*, 442–444.
14. Jenne, A., and Famulok, M. (1998). A novel ribozyme with ester transferase activity. Chem. Biol. *5*, 23–34.
15. Illangasekare, M., Sanchez, G., Nickles, T., and Yarus, M. (1995). Aminoacyl-RNA synthesis catalyzed by an RNA. Science *267*, 643–647.
16. Lee, N., Bessho, Y., Wei, K., Szostak, J.W., and Suga, H. (2000). Ribozyme-catalyzed tRNA aminoacylation. Nat. Struct. Biol. *7*, 28–33.
17. Li, N., and Huang, F. (2005). Ribozyme-catalyzed aminoacylation from CoA thioesters. Biochemistry *44*, 4582–4590.
18. Sengle, G., Eisenführ, A., Arora, P.S., Nowick, J.S., and Famulok, M. (2001). Novel RNA catalysts for the Michael reaction. Chem. Biol. *8*, 459–473.
19. Conn, M.M., Prudent, J.R., and Schultz, P.G. (1996). Porphyrin metalation catalyzed by a small RNA molecule. J. Am. Chem. Soc. *118*, 7012–7013.
20. Li, Y., and Sen, D. (1996). A catalytic DNA for porphyrin metallation. Nat. Struct. Biol. *3*, 743–747.
21. Wilson, C., and Szostak, J.W. (1995). In vitro evolution of a self-alkylating ribozyme. Nature *374*, 777–782.
22. Wecker, M., Smith, D., and Gold, L. (1996). In vitro selection of a novel catalytic RNA: characterization of a sulfur alkylation reaction and interaction with a small peptide. RNA *2*, 982–994.
23. Johnston, W.K., Unrau, P.J., Lawrence, M.S., Glasner, M.E., and Bartel, D.P. (2001). RNA-catalyzed RNA polymerization: accurate and general RNA-templated primer extension. Science *292*, 1319–1325.
24. Tarasow, T.M., Tarasow, S.L., and Eaton, B.E. (1997). RNA-catalysed carbon-carbon bond formation. Nature *389*, 54–57.
25. Seelig, B., and Jäschke, A. (1999). A small catalytic RNA motif with Diels-Alderase activity. Chem. Biol. *6*, 167–176.
26. Tuerk, C., and Gold, L. (1990). Systematic evolution of ligands by exponential enrichment: RNA ligands to bacteriophage T4 DNA polymerase. Science *249*, 505–510.
27. Ellington, A.D., and Szostak, J.W. (1990). In vitro selection of RNA molecules that bind specific ligands. Nature *346*, 818–822.
28. Robertson, D.L., and Joyce, G.F. (1990). Selection in vitro of an RNA enzyme that specifically cleaves single-stranded DNA. Nature *344*, 467–468.
29. Marsh, J.J., and Lebherz, H.G. (1992). Fructose-bisphosphate aldolases: an evolutionary history. Trends Biochem. Sci. *17*, 110–113.
30. Fessner, W.-D., Schneider, A., Held, H., Sinerius, G., Walter, C., Hixon, M., and Schloss, J.V. (1996). The mechanism of class II, metal-dependant aldolases. Angew. Chem. Int. Ed. Engl. *35*, 2219–2221.
31. Hixon, M., Sinerius, G., Schneider, A., Walter, C., Fessner, W.D., and Schloss, J.V. (1996). Quo vadis photorespiration: a tale of two aldolases. FEBS Lett. *392*, 281–284.
32. Morse, D.E., and Horecker, B.L. (1968). The mechanism of action of aldolases. Adv. Enzymol. Relat. Areas Mol. Biol. *31*, 125–181.
33. Wagner, J., Lerner, R.A., and Barbas, C.F., 3rd. (1995). Efficient aldolase catalytic antibodies that use the enamine mechanism of natural enzymes. Science *270*, 1797–1800.
34. Hoffmann, T., Zhong, G.F., List, B., Shabat, D., Anderson, J., Gramatikova, S., Lerner, R.A., and Barbas, C.F., 3rd. (1998). Aldolase antibodies of remarkable scope. J. Am. Chem. Soc. *120*, 2768–2779.
35. Jaschke, A. (2001). RNA-catalyzed carbon-carbon bond formation. Biol. Chem. *382*, 1321–1325.
36. Mandal, M., Lee, M., Barrick, J.E., Weinberg, Z., Emilsson, G.M., Ruzzo, W.L., and Breaker, R.R. (2004). A glycine-dependent riboswitch that uses cooperative binding to control gene expression. Science *306*, 275–279.
37. List, B., Lerner, R.A., and Barbas, C.F., 3rd. (2000). Proline-catalyzed direct asymmetric aldol reactions. J. Am. Chem. Soc. *122*, 2395–2396.
38. List, B., Hoang, L., and Martin, H.J. (2004). New mechanistic studies on the proline-catalyzed aldol reaction. Proc. Natl. Acad. Sci. USA *101*, 5839–5842.
39. Mathews, D.H., Sabina, J., Zuker, M., and Turner, D.H. (1999). Expanded sequence dependence of thermodynamic parameters improves prediction of RNA secondary structure. J. Mol. Biol. *288*, 911–940.